

Removal Studies of S^{2-} Based on SBA-15-Pb(II) Composite

Xiao-Dong, Li

Department of Basic Science, Jilin Jianzhu University, 5088 Xincheng Street, Changchun 130118,
Jilin Province, P.R. CHINA

Qing-Zhou, Zhai*⁺

Research Center for Nanotechnology Changchun University of Science and Technology, Changchun 130022,
7186 Weixing Road, Jilin Province, P.R. CHINA

ABSTRACT: SBA (Santa Barbara Amorphous)-15 nano mesoporous molecular sieve was successfully synthesized by hydrothermal method and after its adsorption of Pb^{2+} the prepared material was used to adsorb S^{2-} from aqueous solution. The surface and pore structure of SBA-15, the (SBA-15)-Pb(II), and the composite material of S^{2-} adsorbed by the (SBA-15)-Pb(II) were characterized by powder X-Ray Diffraction (XRD), Scanning Electron Microscopy (SEM) and low-temperature nitrogen adsorption-desorption isotherm. The effects of solution acidity, S^{2-} concentration, contact time, and temperature on the adsorption of S^{2-} by the (SBA-15)-Pb(II) were investigated. The optimized adsorption conditions were obtained. The adsorption rate for S^{2-} by the (SBA-15)-Pb(II) reached 96.33 %. The change of Gibbs free energy in the adsorption process, $\Delta G^{\circ} < 0$, can judge that the adsorption process is spontaneous. The enthalpy change in the adsorption process is less than zero, showing that the adsorption process is an exothermic reaction. The negative value of entropy change indicates that the adsorption process is a process of entropy reduction. The adsorption of S^{2-} by the (SBA-15)-Pb(II) belongs to the pseudo-second-order kinetics. Freundlich isothermal adsorption equation can better describe the adsorption process. A novel method has been developed to adsorb S^{2-} from wastewater.

KEYWORDS: S^{2-} ; Pb^{2+} ; SBA-15 nano mesoporous molecular sieve; Adsorption; Sulfur pollution; Freundlich; Pseudo-second order; Thermodynamics.

INTRODUCTION

Air pollution, water pollution and soil pollution prevention, and ecological restoration are important research indexes of environmental control [1-11]. In industrial areas, sulfur pollution is one of the main sources of air, water, and soil pollution [12,13]. The sources of S^{2-} pollution in water are numerous, including various discharged sulfates. These sulfates will flow into the water environment through various actions, their range of

activities will gradually expand, and finally, they enter the bottom of the water environment to accumulate. The lack of oxygen at the bottom of the water environment makes anaerobic metabolism active because the oxygen content is too low, such as sulfate-reducing bacteria, which facilitates its growth. As a result of the metabolism of sulfate-reducing bacteria, the sulfate ion will be converted into sulfur ions and other substances. There are a large

* To whom correspondence should be addressed.

+ E-mail: zhaiqingzhou@163.com

1021-9986/2022/9/3007-3019

13\$/6.03

number of organisms living in the water environment, their metabolic process can not be separated from the existence of metal ions. Because of the existence of sulfur-containing substances and their high activity in reacting with metal ions, it is difficult for organisms in water to obtain some necessary metal elements, resulting in a large number of deaths of aquatic organisms. It causes great harm to the ecological balance of water bodies. Because of the wide distribution of sulfur, it is very difficult to administer it. Several commonly used methods to solve sulfur pollution have been studied, including the chemical method, physical adsorption method, physicochemical method, electrochemical method, and so on [12-15]. Adsorption has been reported to be a strategic method in solving various pollution problems, such as heavy metals [8], including sulfur pollution [16,17]. The adsorption method is especially suitable for solving the sulfur pollution problem and has many advantages, so it has become the focus and hot spot of research.

A porous molecular sieve is a class of materials with selective adsorption properties, large specific surface area, strong adsorption capacity, and uniform pore size distribution [7]. Compared with traditional microporous materials, nano-mesoporous materials have a high specific surface area and good adsorption performance. SBA-15 mesoporous molecular sieve is a new emerging class of nanomaterials [18,19]. Because of its high hydrothermal stability, large pore size, and specific surface area, SBA-15, and other mesoporous molecular sieve materials have been studied in many new fields, especially in the fields of adsorption and separation and higher inorganic materials [20-22].

In this study, mesoporous silica SBA-15 was prepared using Pluronic P123 copolymer as the structure-directing agent and TEOS as the silica precursor by hydrothermal method and modified with Pb^{2+} to adsorb S^{2-} in aqueous solution to remove harmful sulfur ions in the environment. The experimental conditions of adsorption of Pb^{2+} by SBA-15 have previously been studied in detail [23]; on this basis, the optimal adsorption conditions of S^{2-} in aqueous phase by the (SBA-15)-Pb(II) adsorption have been explored to study the desulfurization performance. The kinetic, thermodynamic, and adsorption isotherm properties of the adsorption process have been investigated in the hope of advancing the prevention and control of sulfur pollution. This method can not only adsorb the

harmful Pb^{2+} ions [23], but also remove harmful substances S^{2-} , which has a very high application value. A new method for S^{2-} adsorption was established.

EXPERIMENTAL SECTION

Chemicals

Triblock copolymer, polyethylene glycol-block-polypropylene glycol-block-polyethylene glycol (P123) came from Aldrich. Ethyl orthosilicate (TEOS) was purchased from Shanghai Reagent Factory, China. Concentrated hydrochloric acid (12 mol/L) was obtained from Beijing Chemical Plant, China. Sodium sulfide nonahydrate ($\text{Na}_2\text{S}\cdot 9\text{H}_2\text{O}$), lead nitrate, and sodium hydroxide were produced in Beijing Chemical Plant, China. The reagents used in the experiment were analytically pure and water was deionized water.

Instruments

The information on crystal phase structure and periodic arrangement was determined by a D5005 X-ray diffractometer (Siemens, Germany), with Cu-K α target, $\lambda = 1.540560 \text{ \AA}$, operating voltage 50 kV, operating current (tube current) 150 mA. The scan range was $0.4^\circ \sim 10^\circ$ and the step size was $0.02^\circ/\text{step}$. Scanning Electron Microscopy (SEM) images were taken using a Philips XL30 field emission scanning electron microscope to observe the particle morphology and size of the sample. The sample was prepared by using ethanol. The sample was dropped onto the slide for conducting layer treatment and the operating voltage was 20 kV. At 77 K liquid nitrogen temperature, the pore structure parameters of molecular sieve materials such as N_2 adsorption-desorption isothermal curve and specific surface area were determined by a Micromeritics ASAP2010M adsorption analyzer. The specific surface area was calculated using the BET (Brunner-Emmett-Teller) method [24], while the pore size distribution was calculated using the BJH (Barrett-Joyner-Halenda) equation [25]. The relevant data involved in the calculation of each parameter were obtained according to the adsorption branch of nitrogen adsorption-desorption isotherms of each sample prepared experimentally. S^{2-} was determined by Ag_2S gravimetric subtraction method.

Synthesis of SBA-15 adsorbent

Hydrothermal synthesis SBA-15 was used and the details are as follows:

P123 triblock copolymer template of 2 g was dissolved in 15 g deionized water and 60 g 2 mol/L of hydrochloric acid solution. 4.25 g TEOS were gradually added to the mixed solution at 40°C and continuous stirring for 24 h. Then, the mixed solution was added to the reactor and continuously crystallized at 100 °C for 48 h. The prepared product was dried at room temperature and white powder was obtained. The obtained powder was calcined at a relatively high temperature of 550 °C [26].

(SBA-15)-Pb(II) preparation

$Pb(NO_3)_2$ of 1.5985 g was dissolved in water, 10 mL of concentrated HNO_3 (15.5 mol/L) was added, and the mixture was diluted to 1 L. 40 mL of 1.000 mg/mL Pb^{2+} standard solution was poured into a 100 mL beaker. 0.1 mol/L NaOH solution was used to adjust the solution to pH = 5. 0.1000 g SBA-15 molecular sieve was weighed, placed in the above-mentioned mixed solution, and magnetically stirred for 40 min at room temperature. The resulting product was filtered, washed with deionized water, and dried at room temperature. The obtained product was nominated as (SBA-15)-Pb(II).

Effect of pH on S^{2-} adsorption

A standard working solution of 15 mL of Na_2S solution with 0.20 mg/mL concentration was placed in 50 mL beaker. The desired pHs (9-13) were adjusted with 0.1 mol/L sodium hydroxide and the obtained solution was diluted with distilled water to a volume of 30 mL. A mass of 0.0500 g (SBA-15)-Pb(II) adsorbent was accurately weighed and added to the above-mentioned beaker and stirred for 40 min with a stirring speed of 200 rpm at 25 ± 1 °C. After filtering the suspension in the beaker, the product was dried for 24 h at room temperature. Weighing was made and the weight gain was calculated so as to calculate the adsorption rate and adsorption capacity. pH-adsorption rate curve and pH-adsorption capacity curve were drawn to find the optimal pH.

Effect of S^{2-} solution concentration on adsorption efficiency

Na_2S standard solution of 15 mL of 0.04, 0.10, 0.20, 1.00, 2.00 mg/mL was taken. Water was added to adjust the volume to 30 mL and placed in a 50 mL beaker. The pH solutions were adjusted to 10 using 0.1 mol/L sodium hydroxide solution. Then, the adsorption experiment was

carried out according to the previous method. Weighing was made and its weight gain was calculated so as to calculate its adsorption rate and adsorption capacity. Concentration-adsorption rate curve and concentration-adsorption capacity curve were drawn to find the optimal starting concentration of S^{2-} .

Study on the effect of contact time on S^{2-} adsorption efficiency

Na_2S standard solution of 15 mL of 0.20 mg/mL was taken. Sodium hydroxide solution with a concentration of 0.1 mol/L was respectively added to adjust the pH value of the solution to 10 and water was added to adjust the volume to 30 mL. 0.0500 g (SBA-15)-Pb(II) adsorbent was added in the above-mentioned beaker and stirred for 10, 20, 25, 30, 35, 40, 45, 50 min at 25 ± 1 °C. After filtering the suspension in the beaker, the product was dried for 24 h at room temperature. Weighing was made and its weight gain was calculated so as to calculate its adsorption rate and adsorption capacity. Time-adsorption rate curve was drawn to find the optimal contact time.

Study on the effect of temperature on S^{2-} adsorption efficiency

Na_2S standard solution of 15 mL of 0.20 mg/mL was taken. They were placed in five of 50 mL beakers, respectively. 0.1 mol/L sodium hydroxide solution was respectively added to adjust the pH value of the solution to 10 and water was added to adjust the volume to 30 mL. 0.0500 g (SBA-15)-Pb(II) adsorbent was accurately weighed and added in the above-mentioned beaker and stirred for 40 min at 20, 25, 30, 35, 40 °C. After filtering the suspension in the beaker, the product was dried for 24 h at room temperature. Weighing was made and the weight gain of each sample was calculated so as to calculate the adsorption rate and the adsorption capacity. Temperature-adsorption rate curve was drawn to find the optimal temperature.

Adsorption kinetics equation

Na_2S solution of 15 mL of 0.20 mg/mL was taken and placed in a 50 mL beaker. 0.1 mol/L sodium hydroxide solution was added to adjust the pH value of the solution to 10 and distilled water was added to adjust the volume to 30 mL. (SBA-15)-Pb(II) adsorbent with a mass of 0.0500 g was accurately weighed and added in the above-mentioned

beaker and stirred for 10, 20, 25, 30, 35, 40 min at 25 ± 1 °C on a magnetic stirrer with a stir speed of 200 rpm. After filtering the suspension in the beaker, the product was dried for 24 h at room temperature. Weighing was made and its weight gain was calculated so as to calculate q_e (the adsorption capacity at equilibrium) and q_t (the adsorption capacity at time t). The pseudo-first-order and pseudo-second-order kinetic equations were drawn, respectively, and the corresponding parameters were calculated.

Adsorption thermodynamic equation

Na_2S solution of 15 mL of 0.20 mg/mL was taken and placed in a 50 mL beaker, respectively. 0.1 mol/L sodium hydroxide solution was added to adjust the pH value of the solution to 10 and water was added to adjust the volume to 30 mL. 0.0500 g (SBA-15)-Pb(II) adsorbent was weighed and added in the above-mentioned beaker and stirred for some time at 25, 30, 35, 40, 45 °C on a magnetic stirrer with a stir speed of 200 rpm. After filtering the suspension in the beaker, the product was dried for 24 h at room temperature. Weighing was made and its weight gain was calculated so as to calculate the corresponding concentration and its equilibrium adsorption capacity. The pseudo-first-order and pseudo-second-order kinetic equations were drawn, respectively, and the corresponding parameters were calculated. The fit was carried out using $\ln(q_e/c_e)$ to $1/T$, and the corresponding parameters were calculated.

Adsorption isotherms

(SBA-15)-Pb(II) adsorbent of 0.0500 g was weighed and placed in a 50 mL beaker. 15 mL of 0.040, 0.10, 0.16, 0.20 mg/mL Na_2S solution was added, respectively. 0.1 mol/L sodium hydroxide solution was added to adjust the pH value of the solution to 10 and water was added to adjust volume to 30 mL. The mixture was stirred and contacted for some time at 25, 30, 35, 40, 45 °C on a magnetic stirrer with a stir speed of 200 rpm. After the equilibrium process was achieved, the suspension in the beaker was filtered. The product was dried for 24 h at room temperature. Weighing was made and its weight gain was calculated so as to calculate its equilibrium concentration and equilibrium adsorption capacity. Langmuir adsorption isotherms and Freundlich adsorption isotherms were drawn.

RESULTS AND DISCUSSION

Effect of adsorption condition on adsorption efficiency

Fig. 1 shows a relationship between pH value and S^{2-} adsorption rate (Fig. 1A) or adsorption capacity (Fig. 1B). It can be seen from the figure that from pH 8-10 as the pH value increased, S^{2-} adsorption rate and adsorption capacity increased. When $\text{pH} > 10$, as the pH value increased, S^{2-} adsorption rate and adsorption capacity decreased. At $\text{pH} = 10$, S^{2-} adsorption rate and adsorption capacity are the largest, reaching 96.33% and 57.81 mg/g, respectively. At $\text{pH} > 10$, as the pH value increased, OH^- concentration in the solution increased gradually, and then inhibited S^{2-} adsorption [27-29]. Fig. 2 shows a relationship between the initial concentration of S^{2-} and adsorption rate or adsorption capacity. It can be seen from the figure that the adsorption rate increased with the initial concentration of S^{2-} . The maximum was reached at the initial concentration of 0.1 mg/mL S^{2-} . And the adsorption capacity increased gradually with the increase of the initial concentration of S^{2-} . So the optimal solution concentration is judged by the curves of adsorption rate and adsorption capacity, and the optimal starting concentration was selected to be 0.1 mg/mL. The adsorption was then revealed contact time-dependent (Fig. 3) until the equilibrium was reached (40th minute). The influence of contact time was attributed to the diffusion force, as suggested by other studies [9,10]. Fig. 4 shows a relationship between adsorption temperature and adsorption rate. From the figure, it can be seen that the adsorption rate increased with the increase of temperature. At 25 °C, the maximum was reached and then decreased with increasing temperature. So the optimal adsorption temperature is determined by the adsorption rate curve, and the optimum adsorption temperature was 25 °C. When the temperature was in the range of 25 ~ 45 °C, the adsorption of S^{2-} onto (SBA-15)-Pb(II) at different temperatures showed a decrease in the adsorption rate and capacity with an increase in temperature. The adsorption process was an exothermic reaction.

Property of adsorption system

Kinetics of sorption describing the solute uptake rate which in turn governs the residence time of sorption reaction is one of the important characteristics defining the efficiency of sorption. Hence, in this study, the adsorption kinetic model which is currently commonly used, namely

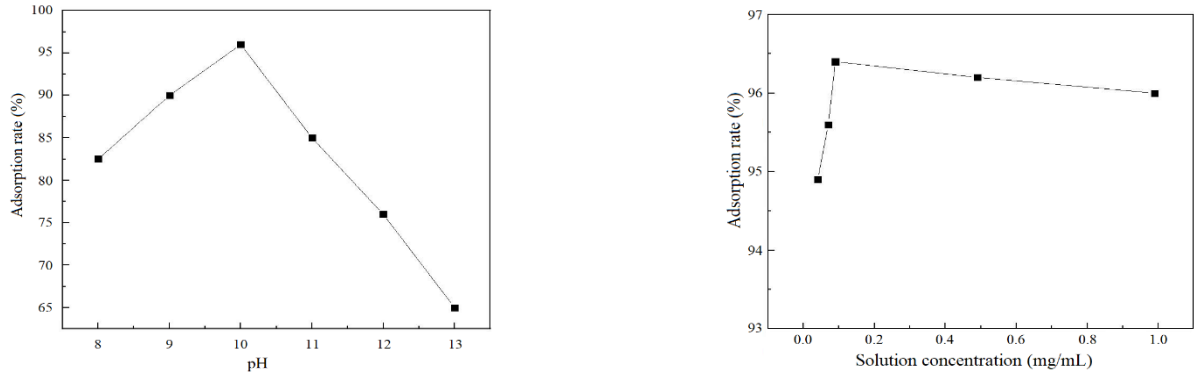


Fig. 1: Effect of pH on S^{2-} adsorption: (A) adsorption rate; (B) adsorption capacity (adsorbent dosage: 1.67 g/L, initial concentration of S^{2-} : 0.1 mg/mL, stirring time: 40 min, temperature: 25°C).

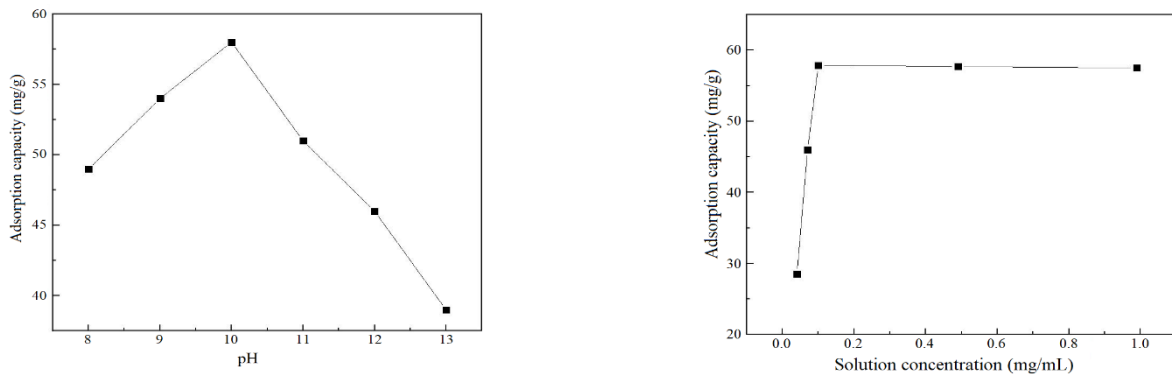


Fig. 2: Effect of initial concentration of solution on adsorption rate of S^{2-} (A) and adsorption capacity (B) (Adsorbent dosage: 1.67 g/L, pH = 10, stirring time: 40 min, temperature: 25°C).

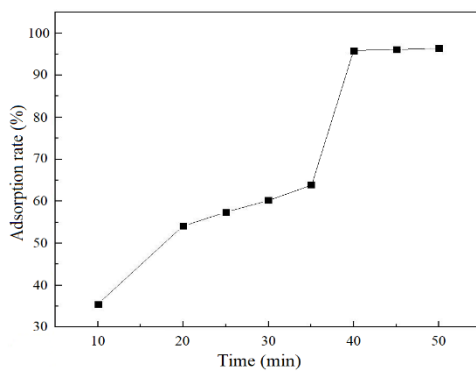


Fig. 3: Effect of contact time on S^{2-} adsorption rate (Adsorbent dosage: 1.67 g/L, pH = 10, initial concentration of S^{2-} : 0.1 mg/mL, temperature: 25°C).

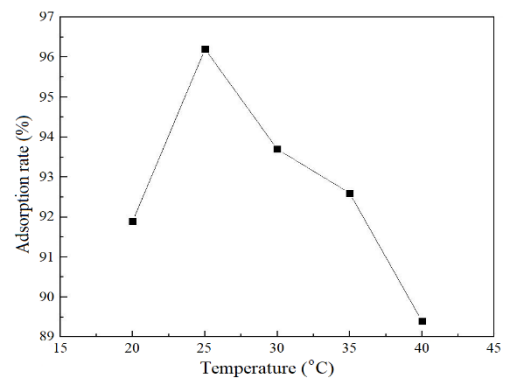


Fig. 4: Effect of temperature on S^{2-} adsorption rate (Adsorbent dosage: 1.67 g/L, pH = 10, contact time: 40 min, initial concentration of S^{2-} : 0.1 mg/mL).

Table 1: Adsorption kinetic parameters.

t (min)	q _t (mg/g)	[q _e -q _t] (mg/g)	ln(q _e -q _t)	t/q _t
10	21.882	35.918	3.581	0.456
20	32.864	24.936	3.216	0.608
25	35.267	22.905	3.131	0.716
30	36.568	21.232	3.055	0.820
35	39.216	18.584	2.922	0.892

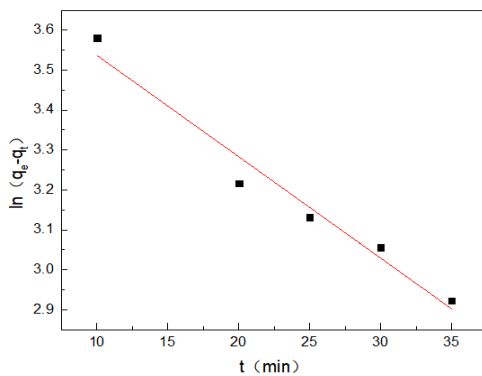


Fig. 5: Pseudo-first-order kinetic equation (Adsorbent dosage: 1.67 g/L, pH =10, S²⁻ initial concentration: 0.1 mg/mL, temperature: 25°C).

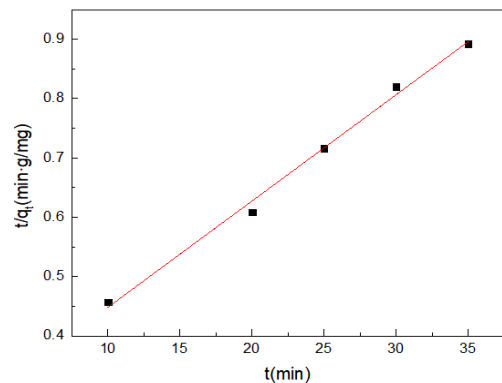


Fig. 6: Pseudo-second-order kinetic equation (adsorbent dosage: 1.67 g/L, pH =10, S²⁻ initial concentration: 0.1 mg/mL, temperature: 25°C).

pseudo-first-order kinetics and pseudo-second-order kinetic adsorption rate model is used to describe the adsorption rate of adsorbent toward solute. The adsorption mechanism of (SBA-15)-Pb(II) toward S²⁻ can be discussed.

The pseudo-first-order kinetic model formula [30,31] is:

$$\ln(q_e - q_t) = \ln q_e - \frac{k_1}{2.303} t \quad (1)$$

The pseudo-second-order dynamic model formula [30,31] is:

$$\frac{t}{q_t} = \frac{1}{k_2 q_e^2} + \frac{t}{q_e} \quad (2)$$

Where q_e (mg/g) is the adsorption equilibrium mass concentration, q_t (mg/g) is the adsorption amount at t time, k_1 is the pseudo-first-order rate constant, and k_2 [g/(mg·min)] is the pseudo-second-order adsorption rate constant [8, 32-34].

According to the experimental data, the adsorption kinetic data are calculated, and the results are shown

in Table 1. The kinetic curves were made according to the calculated data, as shown in Fig. 5 and 6. It was calculated from Eqs. (1) and (2) and obtained that the pseudo-first-order kinetic equation $\ln(q_e - q_t) = -0.02539t + 3.79061$ ($R^2 = 0.9670$), rate constant $k_1 = 0.05851 \text{ min}^{-1}$. The adsorption capacity obtained is $q_e = 44.283 \text{ mg/g}$, which is quite different from that obtained by the experiments.

The rate constant calculated from pseudo-second-order kinetic equation $t/q_t = 0.0179t + 0.26931$ ($R^2 = 0.9947$) was $k_2 = 0.001189 \text{ [g/(mg·min)]}$ and the adsorption capacity was $q_e = 55.866 \text{ mg/g}$. This is not significantly different from the adsorption capacity ($q_e = 57.811 \text{ mg/g}$) value obtained from the experiment. Therefore, the process of adsorption of S²⁻ by (SBA-15)-Pb(II) is considered a pseudo-second-order kinetics [35-39].

Thermodynamic of adsorption

The thermodynamic parameters of adsorption process can be calculated by the following formula [40]:

$$K_d = \frac{q_e}{C_e} \quad (3)$$

Table 2: Thermodynamic parameter of adsorption.

T/(K)	C _e (mg/mL)	q _e (mg/g)	1/T	q _e /C _e	ln(q _e /C _e)
298	0.003667	57.801	0.003354	15762.20344	9.665370
303	0.006205	56.277	0.003298	9069.621273	9.112685
308	0.007258	55.645	0.003245	7666.712593	8.944643
313	0.01527	50.838	0.003193	3329.273084	8.110509
318	0.023385	45.969	0.003143	1965.747274	7.583627

Table 3: ΔG⁰ values at different temperature.

T(K)	298.15	303.15	308.15	313.15	318.15
ΔG ⁰ (kJ/mol)	-24.121305	-23.162370	-22.203435	-21.244500	-20.285565
ΔH ⁰ (kJ/mol)	81.3026	81.3026	81.3026	81.3026	81.3026
ΔS ⁰ (kJ/mol.K)	-191.787	-191.787	-191.787	-191.787	-191.787

$$\Delta G^0 = -RT \ln K_d \quad (4)$$

$$\ln K_d = -\Delta G^0 / RT = -\Delta H^0 / RT + \Delta S^0 / R \quad (5)$$

Where K_d is the adsorption equilibrium constant related to temperature, ΔG^0 is the free energy variable value of the adsorption process (kJ/mol), R is the ideal gas constant (8.314 J/mol.K), T is the absolute temperature (K), ΔH^0 is the enthalpy change of adsorption process (kJ/mol), ΔS^0 is the adsorption entropy change value (J/mol.K).

The adsorption thermodynamic data are calculated according to the experimental data, as shown in Table 2. The thermodynamic curve is made according to the calculated data, as shown in Fig. 7. The enthalpy change $\Delta H^0 = -81.3026$ kJ/mol, entropy change $\Delta S^0 = -191.787$ J/(mol.K) was obtained by calculation. Gibbs free energy change at different temperatures is calculated from the formula $\Delta G^0 = \Delta H^0 - T\Delta S^0$ and the results are shown in Table 3. The calculated ΔG^0 show that the Gibbs free energy changes $\Delta G^0 < 0$ during the adsorption process and it can be judged that the adsorption process is spontaneous. When the temperature is 25 ~ 45 °C, the adsorption is an exothermic entropy reduction reaction process [41, 42].

Adsorption isotherm

Langmuir curve is described by the following Equation [43]:

$$\frac{C_e}{q_e} = \frac{1}{Q_0 b} + \left(\frac{1}{Q_0} \right) C_e \quad (6)$$

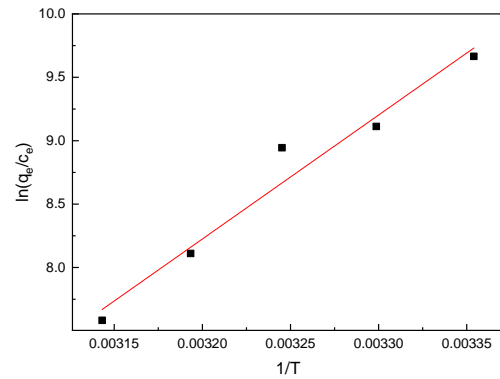


Fig. 7: Thermodynamics equation diagram (Adsorbent dosage: 1.67 g/L, pH = 10, S²⁻ initial concentration: 0.1 mg/mL).

Where C_e (mg/L) is the equilibrium concentration, q_e (mg/g) is the amount of adsorbate adsorbed by adsorbent, and Q_0 and b are Langmuir constants associated with the adsorption ability and the adsorption rate, respectively.

Freundlich linear form equation [44] is:

$$\ln q_e = \ln K_F + \frac{1}{n} \ln C_e \quad (7)$$

Where q_e (mg/g) is the adsorption amount at equilibrium, and C_e (mg/L) is the concentration of adsorbate solution at equilibrium. K_F and n are Freundlich constants. K_F is the adsorption isotherm constant, indicating the degree of adsorption. And $1/n$ represents the adsorption strength. $1/n$ is usually less than 1 because

Table 4: Langmuir isothermal equation data.

T (K)	Equation	q_m (mg/g)	b	R^2
298.15	$C_e/q_e = 0.0455C_e + 0.000224915$	21.95	202.57	0.8917
303.15	$C_e/q_e = 0.1044C_e + 0.000717567$	9.57	588.12	0.8728
308.15	$C_e/q_e = 0.0732C_e + 0.000619709$	13.66	118.13	0.8565

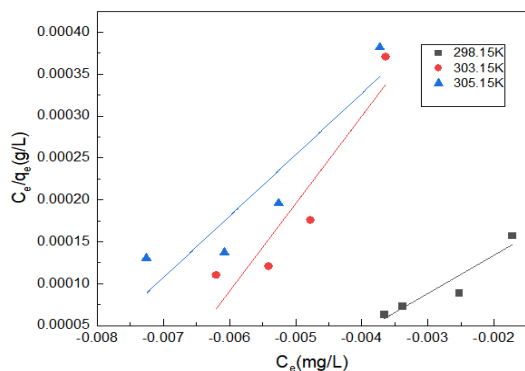


Fig. 8: Langmuir adsorption isotherm (Adsorbent dosage: 1.67 g/L, pH = 10).

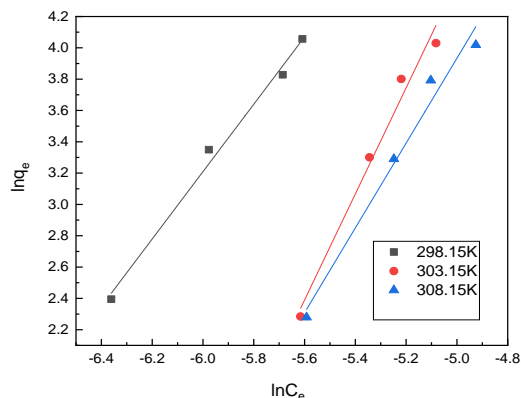


Fig. 9: Freundlich adsorption isotherm (Adsorbent dosage: 1.67 g/L, pH = 10).

mesh with the highest binding energy is utilized first, followed by the weaker mesh in turn.

The fitting curves of Langmuir and Freundlich equations are shown in Fig. 8, 9, and the relevant parameters are listed in Tables 4 and 5. It can be seen that the Freundlich adsorption isotherm equation fits well and has a high correlation coefficient, indicating that the Freundlich model can better describe the adsorption of S^{2-} by (SBA-15)-Pb(II), which is heterogeneous adsorption. Fig. 10 represents the adsorption mechanism of this system. The major reason for this system should be heterogeneous adsorption. The adsorption should be carried out inside the channels of the molecular sieve.

Sample characterization

Fig. 11 shows the XRD figure of the sample. As can be seen from the diagram, there are four distinct diffraction peaks for the mesoporous material SBA-15, corresponding to the diffraction of (100), (110), (200), (210) crystal planes, respectively. With an increase in the number of adsorbed ions Pb^{2+} , S^{2-} , the main characteristic diffraction peak (100) is invariant, which explains that the original skeleton of the SBA-15 has not been destroyed. However, the diffraction of (110), (200), (210) crystal planes

disappeared, indicating that the framework arrangement order of SBA-15 mesoporous materials in the composites decreased or disappeared. Fig. 12 shows the scanning electron microscopic analysis of SBA-15, (SBA-15)-Pb(II), (SBA-15)-Pb(II) adsorption S^{2-} composite. It can be seen from the diagram that the sample has a spike-like structure with grain fibers. Its diameter is approximately 333, 356, 344 nm. As can be seen from the diagram, with an increase in the number of adsorbed ions Pb^{2+} , S^{2-} , the order of the material is reduced. Fig. 13, 14 show the N_2 adsorption-desorption isotherms and pore size distribution patterns for the samples at low temperatures, respectively. Table 6 shows the pore size parameters of the samples and their related structural parameters. As can be seen from the diagram, the N_2 adsorption-desorption isotherms of the three samples belong to the IV type isotherm in the IUPAC classification (Bruno definition) and the H1 hysteresis loops are similar [45], which indicates that they still have mesoporous size and the pore shape of the sample is cylindrical. The three stages of curve adsorption are consistent with the adsorption characteristics of mesoporous materials. With an increase in the number of adsorbed ions Pb^{2+} , S^{2-} , the relative partial pressure range on the adsorption isotherms gradually decreases.

Table 5: Freundlich isothermal equation data.

T (K)	Equation	n	k	R ²
298.15	$\ln q_e = 2.15134 \ln C_e + 16.11742$	0.465	2.779	0.9990
303.15	$\ln q_e = 3.38775 \ln C_e + 21.36095$	0.295	3.062	0.9983
308.15	$\ln q_e = 2.70857 \ln C_e + 17.47635$	0.369	2.861	0.9978

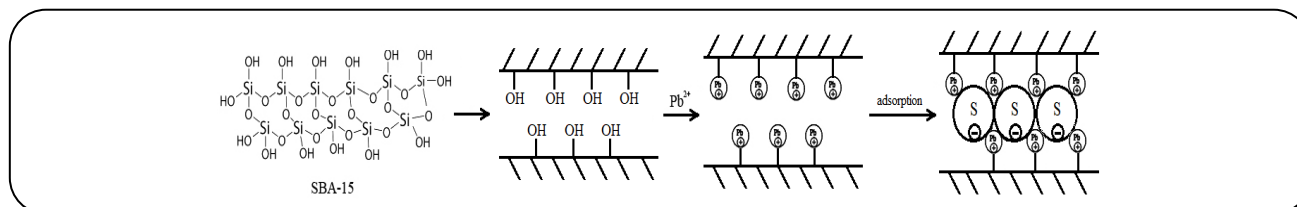


Fig. 10: Mechanism diagram of adsorption.

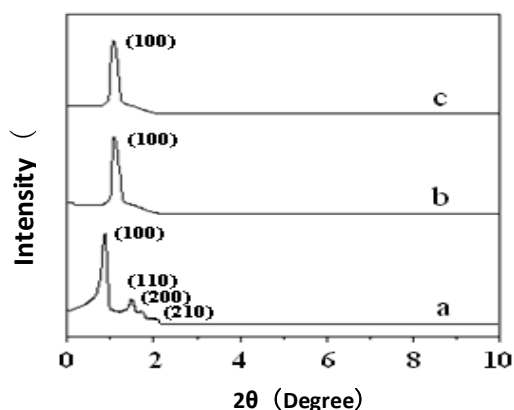


Fig. 11: X-ray diffraction pattern of sample a) SBA-15; b) (SBA-15)-Pb(II); c) (SBA-15)-Pb(II)-S(II).

This is because the Pb^{2+} , S^{2-} in the composite spread into SBA-15 channels, made the channels narrow and the pore volume decrease. The gradual decrease of BET-specific surface area indicates that the Pb^{2+} , S^{2-} has entered the SBA-15 pores rather than adsorbed on the outer surface of the SBA-15. By comparing the pore size distribution of the three samples, it can be seen that with the increase of the number of adsorbed ion Pb^{2+} , S^{2-} the most probable pore diameter is reduced. This is because when the Pb^{2+} , S^{2-} was introduced into the SBA-15 channels, the most probable pore diameter was reduced, indicating that the Pb^{2+} , S^{2-} entered the SBA-15 channels.

Note : cell parameter $a_0 = (2/\sqrt{3})d_{100}$; average pore diameter $D_p = 4V_{mes}/S_{BET}$, V_{mes} mesoporous volume, S_{BET} BET surface area; hole thickness = $a_0 - D_p$

CONCLUSIONS

In the present work, (SBA-15)-Pb(II) adsorbent was used to study the optimal adsorption conditions, thermodynamic and kinetic properties of (SBA-15)-Pb(II) for S^{2-} adsorption and adsorption isotherm equations. The prepared materials have provided new solutions for removing S^{2-} from the aqueous solution.

Under the obtained optimal conditions (the temperature at 25 ± 1 °C, S^{2-} solution volume is 30 mL, pH 10, 0.05 g adsorbent dosage, 0.1 mg/mL initial concentration of Na_2S solution, 40 min contact time), the adsorption rate reaches 96.33 % and the adsorption capacity is 57.811 mg/g.

Adsorption kinetic studies showed that the adsorption of S^{2-} by (SBA-15)-Pb(II) belonged to pseudo-second-order kinetics, the rate constant $k = 0.001189$ g/(mg min), the experimental adsorption capacity $q_e = 57.811$ mg/g, and theoretical adsorption capacity $q_e = 55.866$ mg/g.

The thermodynamic study of adsorption showed that according to the calculated ΔG^0 it can be known that when the temperature is 25 - 45°C, $\Delta G^0 < 0$, the adsorption enthalpy change $\Delta H^0 = -81.3026$ kJ/mol, the adsorption system is exothermic, and the adsorption entropy change $\Delta S^0 = -191.787$ J/(mol·K).

The results of linear fitting of Langmuir and Freundlich isothermal adsorption equations found that the adsorption accords with the isothermal adsorption equation established according to the multi-molecular layer adsorption model, and Freundlich isothermal adsorption equation can better represent the adsorption process. The method for the adsorption of S^{2-} by the

Table 6: Structural parameters of sample holes.

Sample	Spacing of crystal face, d_{100} (nm)	Cellular parameter, a_0 (nm)	Hole thickness (nm)	BET surface area (m^2/g)	Mesoporous volume (cm^3/g)	Average hole diameter, D_p (nm)
SBA-15	10.26	11.85	4.15	613	1.04	7.70
(SBA-15)-Pb(II)	10.33	10.76	3.42	555	0.91	7.34
(SBA-15)-Pb(II)-S(II)	8.99	10.39	3.15	510	0.89	7.24

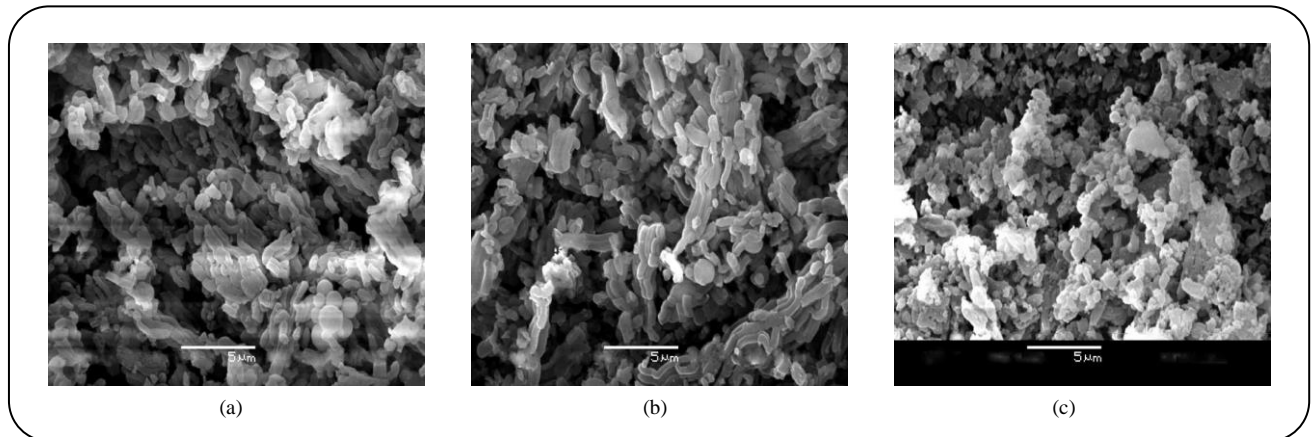


Fig. 12: SEM of samples, a) SBA-15; b) (SBA-15)-Pb(II); c) (SBA-15)-Pb(II)-S(II).

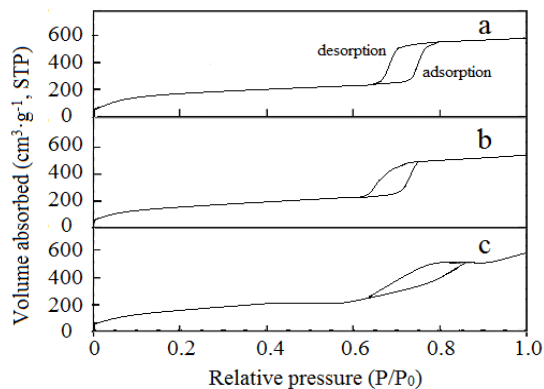
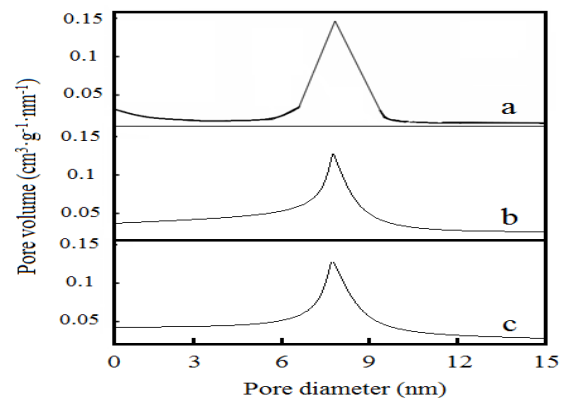
Fig. 13: N_2 adsorption-desorption curve of sample at low temperature, a) SBA-15; b) (SBA-15)-Pb(II); c) (SBA-15)-Pb(II)-S(II).

Fig. 14: Pore size distribution of Sample, a) SBA-15; b) (SBA-15)-Pb(II); c) (SBA-15)-Pb(II)-S(II).

(SBA-15)-Pb(II) is likely to become a very viable alternative to other traditional treatment methods.

Acknowledgments

This study was supported by the Science Research Project of the Education Department, Jilin Province from the 13th Five-Year Plan (JJKH20200265KJ).

Received : Aug. 28, 2021 ; Accepted : Nov. 17, 2021

REFERENCES

- [1] de Freitas G.R., da Silva M.G.C., Vieira M.G.A., Biosorption Technology for Removal of Toxic Metals: A Review of Commercial Biosorbents and Patents, *Environ. Sci. Pollut. Res.*, **26**: 19097-19118 (2019).
- [2] Siya A.A., Shamsuddin M.R., Low A., Rabat N.E., A Review on Recent Developments in the Adsorption of Surfactants from Wastewater, *J. Environ. Manage.*, **254**: 109797 (2020).

- [3] Zahra B., Hossein A., [Kinetic and Thermodynamic Study of Chromium Picolinate Removing from Aqueous Solution onto the Functionalized Multi-Walled Carbon Nano Tubes](#), *Iran. J. Chem. Chem. Eng.(IJCCCE)*, **40**:765-779 (2021).
- [4] Ramezani F., Zare-Dorabei R., [Simultaneous Ultrasonic-Assisted Removal of Malachite Green and Methylene Blue from Aqueous Solution by Zr-SBA-15](#), *Polyhedron*, **166**:153-161 (2019).
- [5] Liu C., Zeng S.L., Yang B.Q., Jia F.F., Song S.X., [Simultaneous Removal of \$Hg^{2+}\$, \$Pb^{2+}\$ and \$Cd^{2+}\$ from aqueous solutions on multifunctional \$MoS_2\$](#) , *J. Mol. Liq.*, **296**: 111987 (2019).
- [6] Badi M.Y., Esrafil A. Kalantary R.R., Azari A., Ahmadi E., Gholami M., [Removal of Diethyl Phthalate from Aqueous Solution Using Persulfate-Based \(\$UV/Na_2S_2O_8/Fe^{2+}\$ \) Advanced Oxidation Process](#), *J. Mazandaran Univ. Med. Sci.*, **25**: 122-135 (2015).
- [7] Sabri, A.A., Albayati, T.M., Alazawi, R.A., [Synthesis of Ordered Mesoporous SBA-15 and Its Adsorption of Methylene Blue](#), *Korean J. Chem. Eng.*, **32**: 1835-1841 (2015).
- [8] Rahmi R., Iqhrammullah M., Audina U., Husin H., Fathana H., [Adsorptive Removal of Cd\(II\) Using Oil Palm Empty Fruit Bunch-Based Charcoal/Chitosan-EDTA Film Composite](#), *Sustain. Chem. Pharm.*, **21**: 100449 (2021).
- [9] Marlina, Iqhrammullah M., Darmadi, Mustafa I., Rahmi, [The Application of Chitosan Modified Polyurethane from Adsorbent](#), *Rasa. J. Chem.*, **12**: 494-501 (2019).
- [10] Marlina, Iqhrammullah M., Saleha S., Fathurrahmi, Maulina F.P., Idroes R., [Polyurethane Film Prepared from Ball-Milled Algal Polyol Particle and Activated Carbon Filler for \$NH_3-N\$ Removal](#), *Heliyon*, **6**: e04590 (2020).
- [11] Iqhrammullah M., Marlina., Nus S., [Adsorption Behaviour of Hazard Dye \(Methyl Orange\) on Cellulose-Acetate Polyurethane Sheet](#), *IOP Conf. Ser.: Mater. Sci. Eng.*, **845**: 012035 (2020).
- [12] Castillo X., Pizarro J., Ortiz C., Cid H., Flores M., Canck E.D., Voort. P.V.D., [A Cheap Mesoporous Silica from Fly Ash as An Outstanding Adsorbent for Sulfate in Water](#), *Micropor. Mesopor. Mater.*, **272**: 184-192 (2018).
- [13] Chang X.Q., Wang W.S., Liu B.S., Huang L.Z., Subhan F., [One-Step Strategic Synthesis of x%Ni- \$AlSBA-15\$ Sorbents and Properties of High Adsorption Desulfurization for Model and Commercial Liquid Fuels](#), *Micropor. Mesopor. Mater.*, **268**: 276-284 (2018).
- [14] Nancucheo I., Johnson D.B., [Removal of Sulfate from Extremely Acidic Mine Waters Using Low pH Sulfidogenic Bioreactors](#), *Hydrometallurgy*, **150**:222-226 (2014).
- [15] Diagboya P.N.E., Dikio E.D., [Silica-Based Mesoporous Materials; Emerging Designer Adsorbents for Aqueous Pollutants Removal and Water Treatment](#), *Micropor. Mesopor. Mater.*, **266**: 252-267 (2018).
- [16] Baumann A.E., Aversa G.E., Roy A., FalkM.L., Bedford N.M., Thoi V.S., [Promoting Sulfur Adsorption Using Surface Cu Sites in Metal-Organic Frameworks for Lithium Sulfur Batteries](#), *J. Mater. Chem. A.*, **6**: 4811-4821 (2018).
- [17] Abbasi A., Sardroodi J.J., [The Adsorption of Sulfur Trioxide and Ozone Molecules on Stanine Nanosheets Investigated by DFT: Application to Gas Sensor Devices](#), *Phy. E. L. Dim. Sys. Nano.*, **108**: 382-390 (2019).
- [18] Wang X., Ma X., Song C., Locke D.R., SiefertS., Winana R.E., Mollmer J., Lange M., Moller A., Glaser R., [Molecular Basket Sorbents Polyethylenimine-SBA-15 for \$CO_2\$ Capture from Flue Gas: Characterization and Sorption Properties](#), *Micropor. Mesopor. Mater.*, **169**: 103-111 (2013).
- [19] Nandi M., Mondal J., Sarkar K., Yamauchi Y., Bhaumik A., [Highly Ordered Acid Functionalized SBA-15: A Novel Organocatalyst for the Preparation of Xanthenes](#), *Chem. Commun.*, **47**: 6677-6679 (2011).
- [20] Ding Y., Lu X.R., Dan H., Yuan S.B., Mao X.L., [Controllable Synthesis of Mesoporous Materials and Its Application in Nuclear Industry](#), *Materials Reports*, **28**: 38-41 (2014).
- [21] Zahedi S.S., Larki A., Saghanezhad S.J., Nikpour Y., [1,4-Diazabicyclo \[2.2.2\] Octane Functionalized Mesoporous Silica SBA-15 \(SBA-15@DABCO\): A Novel Highly Selective Adsorbent for Selective Separation/Preconcentration of Cr\(VI\) from Environmental Water Samples](#), *Silicon* (2021).

- [22] Larki A., Saghanezhad S.J., Ghomi M., [Recent Advances of Functionalized SBA-15 in the Separation/Preconcentration of Various Analytes: A Review](#), *Microchem. J.*, **169**: 106601 (2021).
- [23] Ma Y.Q., Zhai Q.Z., Yu H., Yang M.J., [Removal of Pb\(II\) from Water Using Nanoscale SBA-15](#), *Asian J. Chem.*, **23**: 5016-5024 (2011).
- [24] Brunauer S., Emmett P.H., Teller E., [Adsorption of Gases in Multimolecular Layers](#), *J. Am. Chem. Soc.*, **60**: 309-319 (1938).
- [25] Barrett E.P., Joyner L.G., Halenda P.P., [The Determination of Pore Volume and Area Distributions in Porous Substances. I. Computations from Nitrogen Isotherms](#), *J. Am. Chem. Soc.*, **73**: 373-350 (1951).
- [26] Zhai Q.Z., Wu Y.Y., Wang X.H., [Synthesis, Characterization and Sustaining Controlled Release Effect of Mesoporous SBA-15/Ramipril Composite Drug](#), *J. Incl. Phenom. Chem.*, **76**: 300-303 (2013).
- [27] Boukoussa B., Hakiki A., Moulai S., Chikh K., Kherroub D.E., Bouhadjar L., Guedal D., Messaoudi K., Mokhtar F., Hamarcha R., [Adsorption Behaviors of Cationic and Anionic Dyes from Aqueous Solution on Nanocomposite Polypyrrole/SBA-15](#), *J. Mater. Sci.*, **53**: 7372-7386 (2018).
- [28] Mirzaie M., Rashidi A., Tayebi H.A., Yazdanshenas M.E., [Removal of Anionic Dye from Aqueous Media by Adsorption onto SBA-15/Polyamidoamine Dendrimer Hybrid: Adsorption Equilibri and Kinetics](#), *J. Chem. Eng. Data*, **62**: 1365-1376 (2017).
- [29] Hachemaoui M., Boukoussa B., Jsmail I., Mokhtar A., Taha I., Iqbal J., Hacini S., Bengueddach A., Hamacha R., [CuNPs-Loaded Amines-Functionalized-SBA-15 as Effecton Catalysts for Catalytic Reduction of Cationic and Anionic Dyes](#), *Colloid. Surface. A: Physicochem. Engin. Aspect.*, **623**: 123729 (2021).
- [30] Rudzinski W., Plazinski W., [Kinetics of Solute Adsorption at Solid/Solution Interfaces: A Theoretical Development of the Empirical Pseudo-First and Pseudo-Second Order Kinetic Rate Equations, Based on Applying the Statistical Rate Theory of Interfacial Transport](#), *J. Phys. Chem. B*, **110**: 16514-16525 (2006).
- [31] Tian G., Geng J.X., Jin Y.D., Wang C.L., Li S.Q., Chen Z., Wang H., Zhao Y.S., Li S.J., [Sorption of Uranium\(VI\) Using Oxime-Grafted Ordered Mesoporous Carbon CMK-5](#), *J. Hazard. Mater.*, **190**: 442-450 (2011).
- [32] Jawad A.H., Abdulhameed A.S., Malek N.N.A., ALOthman Z.A., [Statistical Optimization and Modeling for Color Removal and COD Reduction of Reactive Blue 19 Dye by Mesoporous Chitosan-Epichlorohydrin/Kaolin Clay Composite](#), *Inter. J. Biol. Macromol.*, **164**: 4218-4230 (2020).
- [33] Jawad, A.H., Abdulhameed, A.S., [Statistical Modeling of Methylene Blue Dye Adsorption by High Surface Area Mesoporous Activated Carbon from Bamboo Chip using KOH-Assisted Thermal Activation](#), *Energ. Ecol. Environ.*, **5**: 456-469 (2020).
- [34] Abdulhameed A.S., Mohammad A.T., Jawad A.H., [Modeling and Mechanism of Reactive Orange 16 Dye Adsorption by Chitosan-Glyoxal/TiO₂ Nanocomposite: Application of Response Surface Methodology](#), *Desalin. Water Treat.*, **164**: 346-360 (2019).
- [35] Jawad A.H., Kadhun A.M., Ngoh Y.S., [Applicability of Dragon Fruit \(Hylocereus Polyrhizus\) Peels as Low-Cost Biosorbent for Adsorption of Methylene Blue from Aqueous Solution: Kinetics, Equilibrium and Thermodynamics Studies](#), *Desalin. Water Treat.*, **109**: 231-240 (2018).
- [36] Jawad A.H., Mohammed I.A., Abdulhameed A.S., [Tuning of Fly Ash Loading into Chitosan-Ethylene Glycol Diglycidyl Ether Composite for Enhanced Removal of Reactive Red 120 Dye: Optimization Using the Box-Behnken Design](#), *J. Polym. Environ.*, **28**: 2720-2733 (2020).
- [37] Surip S.N., Abdulhameed A.S., Garba Z.N., Syed-Hassan S.S.A., Ismail K., Jawad A.H., [H₂SO₄-Treated Malaysian Low Rank Coal for Methylene Blue Dye Decolourization and Cod Reduction: Optimization of Adsorption and Mechanism Study](#), *Surf. Interfaces*, **21**: 100641 (2020).
- [38] Jawad A.H., Bardhan M., Islam M.A., Islam M.A., Syed-Hassan S.S.A., Surip S.N., ALOthman Z.A., Khan M.R., [Insights into the Modeling, Characterization and Adsorption Performance of Mesoporous Activated Carbon from Corn Cob Residue via Microwave-Assisted H₃PO₄ activation](#), *Surf. Interfaces*, **21**: 100688 (2020).

- [39] Reghioua A., Barkat D., Jawad A.H., Abdulhameed A.S., Khan M.R., [Synthesis of Schiff's Base Magnetic Crosslinked Chitosan-Glyoxal/ZnO/Fe₃O₄ Nanoparticles for Enhanced Adsorption of Organic Dye: Modeling and Mechanism Study](#), *Sustain. Chem. Pharm.*, **20**: 100379 (2021).
- [40] Singha B., Das S.K., [Adsorption Removal of Cu\(II\) from Aqueous Solution and Industrial Effluent Using Natural/Agricultural Wastes](#), *Colloids Surf. B: Biointerfaces*, **107**: 97-106 (2013).
- [41] Myneni V.R., Kanidarapu N.R., Vangalapati M., [Methylene Blue Adsorption by Magnesium Oxide Nanoparticles Immobilized with Chitosan \(CS-MgONP\): Response Surface Methodology, Isotherm, Kinetics and Thermodynamic Studies](#), *Iran. J. Chem. Chem. Eng. (IJCCE)*, **39**: 29-42 (2020).
- [42] Singha B., Das S.K., [Adsorption Removal of Cu\(II\) from Aqueous Solution and Industrial Effluent Using Natural/Agricultural Wastes](#), *Colloids Surf. B: Biointerfaces*, **107**: 97-106 (2013).
- [43] Langmuir I., [The Constitution and Fundamental Properties of Solids and Liquids. Part I. Solids.](#), *J. Am. Chem. Soc.*, **38**: 2221-2295 (1916).
- [44] Freundlich H., [Adsorption in solution](#), *Phys. Chem. Soc.*, **40**: 1361-1368 (1906).
- [45] Sing K.S.W., Everett D.H., Haul R.A.W., Moscou L., Pierotti R.A., Rouquerol J., Siemieniowska T., [Reporting Physisorption Data for Gas/Solid Systems](#), *Pure. Appl. Chem.*, **87**: 603-606 (1957).